Cellular/Molecular

IP_3 Receptors and Associated Ca^{2+} Signals Localize to Satellite Cells and to Components of the Neuromuscular Junction in Skeletal Muscle

Jeanne A. Powell,[†1] Jordi Molgó,[2] Dany S. Adams,[1] Cesare Colasante,[2] Aislinn Williams,[1] MacKenzie Bohlen,[1] and Enrique Jaimovich[3]

[1]Department of Biological Sciences, Smith College, Northampton, Massachusetts 01063, [2]Laboratoire de Neurobiologie Cellulaire et Moléculaire, Unité Propre de Recherche 9040, Institut Fédératif de Neurobiologie Alfred Fessard, Centre National de la Recherche Scientifique, 91198-Gif sur Yvette cedex, France, and [3]Centro de Estudios Moleculares de la Célula, Instituto de Ciencias Biomédicas, Facultad de Medicina, Universidad de Chile, Casilla 70005, Santiago 6530499, Chile

Recently, we described an inositol 1,4,5-trisphosphate (IP_3) signaling system in cultured rodent skeletal muscle, triggered by high K^+ and affecting gene transcription (Powell et al., 2001). Now, in a study of adult rodent skeletal muscle, using immunocytology and confocal microscopy, we have found a high level of IP_3 receptor (IP_3R) staining in satellite cells, which have been shown recently to contribute to nuclei in adult fibers after muscle exercise. These IP_3R staining cells are positively identified as satellite cells by their position, morphology and staining with satellite-cell-specific antibodies such as desmin and neural cell adhesion molecule. IP_3Rs are also localized to postsynaptic components of the neuromuscular junction (NMJ), in areas surrounding the nuclei of the motor end plate, and in perisynaptic Schwann cells, and localized close to nicotinic acetylcholine receptors of the endplate gutters. Ca^{2+} imaging experiments show calcium release at the motor endplate upon K^+ depolarization precisely in these IP_3R-rich regions. We suggest that electrical activity stimulates IP_3-associated Ca^{2+} signals that may be involved in gene regulation in satellite cells and in elements of the NMJ, contributing both to muscle fiber growth and stabilization of the NMJ.

Key words: **subsynaptic nuclei; fundamental nuclei; perisynaptic Schwann cells; Ca^{2+} signals; gene expression; nerve–muscle interaction**

Introduction

Growth, stabilization, and regeneration of skeletal muscle depends on many elements, such as growth factors, (Doumit et al., 1993; Haugk et al., 1995; Bhasin et al., 1996; Bischoff 1997), neurotrophic factors (for review, see Sanes and Lichtman, 1999; Schaeffer et al., 2001), gliotrophic factors (Trachtenberg and Thompson, 1997), and electrical activity of muscle (Brevet et al., 1976). Strenuous activity and/or tissue damage can cause hypertrophy of muscle because of the activation, multiplication, and fusion of muscle satellite cells (MSCs) with myofibers (for review, see Hawke and Garry, 2001). MSC activation also plays a role in muscle growth after minimal exercise (Kadi and Thornell, 2000), probably without muscle damage. The reaction of MSCs to such muscle activity would probably not involve factors triggered by damage (e.g., growth factors) but could relate to muscle depolarization. Little is known concerning signal transduction pathways involved in muscle growth in response to activity (but cf. Dunn et al., 2000; Pallafacchina et al., 2002). By localizing inositol 1,4,5-trisphosphate receptors (IP_3Rs) and depolarization-triggered calcium transients in cells identified as MSCs, we propose an IP_3-mediated pathway.

At the neuromuscular junction (NMJ) three elements are instrumental in the development and stabilization of nerve–muscle associations: the presynaptic nerve endings, the subsynaptic nuclei of the muscle fiber (for review, see Sanes and Lichtman, 1999; Schaeffer et al., 2001), and the perisynaptic Schwann cells (PSCs) (Rochon et al., 2001). Not yet well explored is the possible role of neuromuscular activity mediated via an IP_3 cascade in PSCs, and in the postsynaptic elements of the NMJ. The well documented IP_3/Ca^{2+} cascade in some cells contributes to different Ca^{2+} signaling patterns (single transients, repetitive oscillations, or sustained plateaus), which can encode specific cellular responses (Dolmetsch et al., 1997). In cultured muscle, Ca^{2+} release from internal stores may follow more than one set of kinetics and may have multiple functions. One of us has described the complex Ca^{2+} release induced by elevated K^+ and constructed a model

Received Dec. 16, 2002; revised May 22, 2003; accepted July 8, 2003.

This work was made possible in part by a Programme d'Évaluation-Orientation de la Coopération Scientifique avec le Cône Sud des Ministères des Affaires Etrangères, et Ministère de l'Education Nationale de la Recherche et de la Technologie de France-Comisión Nacional de Investigación Científica y Tecnológica (C99B03) exchange program and was supported in part by Fondo de Investigación en Areas Prioritarias Grant 15010006 (E.J.), grants from the Association Française contre les Myopathies (J.M), and a grant from the Blakeslee Fund of Smith College (J.A.P.). We thank Kate Nattrass for fixing and cryostat sectioning of some of the mouse limb muscle and Elke Pravda for the S-100 staining experiments. This paper is dedicated to Jeanne A. Powell, to honor her memory.

†Deceased, Sept. 27, 2002.

Correspondence should be addressed to Dr. Enrique Jaimovich, Instituto de Ciencias Biomédicas, Facultad de Medicina, Universidad de Chile, Casilla 70005, Santiago 6530499, Chile. E-mail: ejaimovi@machi.med.uchile.cl.

D. S. Adams's present address: The Forsyth Institute, Cytokine Biology, 140 The Fenway, Boston, MA 02115.

C. Colasante's present address: Laboratorio de Fisiología de La Conducta, Facultad de Medicina, Universidad de Los Andes, Mérida 5101, Venezuela.

 0270-6474/03/238185-08$15.00/0

involving two components with different kinetics (Jaimovich and Rojas, 1994). The presence of IP_3Rs in cultured muscle (Liberona et al., 1998, Powell et al., 2001) and in adult skeletal muscle (Moschella et al., 1995, Salanova et al., 2002) also suggests a role for IP_3 signals in both nuclear and cytoplasmic compartments; these cascades result in the upregulation of gene activity (Powell et al., 2001, Carrasco et al., 2003). We have proposed an excitation–transcription coupling, IP_3 signaling pathway in cultured muscle, which depends on the voltage sensor of the dihydropyridine receptor (DHPR) (Araya et al., 2003). We show here that IP_3Rs are localized to postsynaptic components of the NMJ, at the postsynaptic gutters, surrounding the subsynaptic nuclei of the motor end plate, and are localized close to acetylcholine receptors (AChRs). Finally, IP_3Rs are found in PSCs and MSCs. Ca^{2+} imaging experiments, using fluo-3 AM, show high K^+-induced release of Ca^{2+} precisely in these IP_3R-rich regions. We suggest that electrical activity stimulates IP_3-associated Ca^{2+} signals in MSCs and components of the NMJ that may be involved in gene regulation, possibly contributing to muscle growth and stabilization of the NMJ.

Materials and Methods

Animals. Experiments were carried out in two laboratories: Centre National de la Recherche Scientifique (CNRS), Gif sur Yvette (France), and at Smith College, Northampton MA. Animals used were either normal random inbred adult Swiss-Webster mice (25–30 gm) (CNRS), or +/+ mice (25–30 gm), from a line inbred strain on a background of ReJ (The Jackson Laboratory, Bar Harbor, ME) (Smith). The animals were housed in the animal care facilities, under standard conditions at a constant temperature of 22°C with a 12 hr light/dark cycle. Food and water were provided *ad libitum*. The mice were killed by dislocation of the cervical vertebrae followed by immediate exsanguination or by CO_2 gas.

Isolated nerve–muscle preparations. Left and right mouse hemidiaphragm muscle preparations were isolated with their associated phrenic nerves. The two hemidiaphragms were separated and each was mounted in a Rhodorsil (Rhône-Poulenc, St. Fons, France)-lined organ bath superfused with a standard physiological solution composed of the following (in mM): 154 NaCl, 5 KCl, 2 $CaCl_2$, 1 $MgCl_2$, 5.0 HEPES, pH 7.4, and 11 glucose. The solution was gassed with pure O_2. All experiments were performed at room temperature (22–24°C).

Immunocytochemistry. Muscles were prepared using two different techniques. For the major study of MSCs, levator auris longus, gastrocnemius, extensor digitorum longus, and soleus muscles were excised, stretched on dental wax, and fixed in 4% paraformaldehyde, 0.2% glutaraldehyde in PBS on ice for 45 min, cryopreserved, and cut into ~10 μm sections on a Leica (Nussloch, Germany) CM1900 cryostat. Frozen sections were processed for aldehyde reduction with $NaBH_4$ in PBS just before permeabilization with a solution of 0.1% saponin/1 mM EGTA/0.2% sodium azide/0.5% normal goat serum in PBS. Antibodies were prepared in this same saponin solution. For the fiber bundle technique used to examine motor end plates, diaphragms were dissected, stretched, and fixed for 45 min in 4% paraformaldehyde and rinsed in PBS, whereas small fiber groups were isolated from the motor endplate region. Excess aldehyde groups were reduced with a 0.1 mM glycine solution and blocked against nonspecific binding and permeabilized in 1% BSA/0.5% Triton X-100 in PBS. Antibodies were made up in this solution.

The primary monoclonal antibodies were: anti-desmin (1:20), anti-α-actinin (1:100), anti-skeletal fast isoform of myosin (1:400) (all from Sigma, St. Louis, MO), anti–neural cell adhesion molecule (anti-N-CAM) (1:2) (Developmental Hybridoma, Iowa City), and anti-glial fibrillary acidic protein (GFAP; 1:50–1:200; Chemicon, Temecula, CA). Affinity Bioreagents (Golden, CO) supplied the anti-IP_3R-1 (type 1 isoform) polyclonal antibody (PA3–901) (1:50), the epitope purified polyclonal antibody (PA1–901) (1:25), and the IP_3R-1 peptide epitope, used at a 10× concentration of the antibody to test the specificity of the primary antibody. Both of these anti-IP_3R antibodies gave reasonable results, but the epitope purified gave cleaner images. Other polyclonal antibodies used were raised against S-100 (1:50; Dako, Carpinteria, CA) and laminin (1:25) (Sigma). AChRs were tagged with rhodamine-conjugated α-bungarotoxin (α-BTX) (1:200–1:400) and nuclei were stained with TOTO-3 (dimeric cyanine nucleic acid stains; 1:400) or propidium iodide red (1:1500) (all from Molecular Probes, Eugene, OR). Goat anti-rabbit and goat anti-mouse IgG secondary antibodies, conjugated to either fluorescein isothiocyanate (FITC, or fluorescein) (1:400) or tetramethylrhodamine isothiocyanate (TRITC, or rhodamine) (1:200) (both from ICN Biochemicals, Costa Mesa, CA) were used and when appropriate anti-mouse IgG_1 FITC-conjugated antibody (Southern Biotechnology, Birmingham, AL) was used. Specimens were mounted with Vectashield antifading mounting medium (Vector Laboratories, Burlingame, CA).

A Leica TCS NT scanning laser confocal microscope (with the argon laser at 488 nm for FITC, krypton at 568 nm for TRITC, and HeNe at 633 nm for TOTO-3) was used, and specimens were viewed through an oil-immersion objective [40×, numerical aperture (NA), 1.25]. To obtain some of the confocal images, TRITC, FITC, and TOTO-3 emissions were collected simultaneously using three photomultiplier tubes, and composite images were created automatically by the software; in other cases the three photomultiplier tubes were operated separately, and digital overlays were created later using Adobe Photoshop. Controls were performed, and the scanner was adjusted, ensuring that FITC signals did not contaminate the TRITC data. The "glow over under" function of the TCS system was used consistently to minimize, to the best of our ability, the possibility that electronic signal amplification would lead to biases in the data. The images reproduced herein were manipulated in Adobe Photoshop to improve clarity; no data were added or deleted by those adjustments.

At the CNRS, double-labeled NMJs were observed either with a confocal multiphoton microscope (Leica TCS SP-2; argon laser at 488 nm for FITC, HeNe laser at 543 nm for TRITC) through an oil-immersion objective (63×, NA, 1.32) or with a Sarastro-2000 laser confocal system (Molecular Dynamics, Sunnyvale, CA).

Calcium signal imaging in endplate regions. For calcium signal imaging, a fraction of the mouse hemidiaphragm, containing endplate regions and tendons, was dissected, stretched, and pinned at its resting length on the Rhodorsil base of the recording chamber (2 ml capacity). Nerve–muscle preparations were incubated in the dark, for 30–40 min, with an oxygenated standard solution containing 4 μM fluo-3 AM (Molecular Probes Europe BV, Leiden, The Netherlands). Fluo-3 was dissolved in DMSO containing 0.02% w/v Pluronic F-127 (BASF, Wyandotte, MI). Preparations were washed out of fluo-3 and rinsed several times with dye-free standard medium before being exposed to an isotonic high K^+ (60 mM) medium.

Two experimental protocols to localize endplate regions were used with equal success. In one procedure, superficial motor nerve fibers and endings were resolved in unstained preparations with bright-field and phase-contrast optics (using a magnification of 400×), by following superficial intramuscular axons to their distal unmyelinated endings. In the second procedure, myelinated axons and motor nerve terminals were stained with 2 μM *N*-(3-triethyl ammoniumpropyl)-4-(p-dibutylaminostyryl) pyridinium, dibromide (FM1-43) for 10–15 min in oxygenated standard medium. Effective staining was consistently obtained provided that the end plate region was cleaned of superficial debris and loose connective tissue and that the muscles were uninjured and well oxygenated. The inability of the FM1-43 dye to penetrate nerve membranes (Betz et al., 1992; Ribchester et al., 1994) and the persistence of the staining, because of its partition only on the outer membrane leaflet, renders this dye particularly useful for locating motor nerve endings, at rest, in endplate regions.

Nerve–muscle preparations loaded with fluo-3 or FM1-43 were imaged with a Sarastro-2000 laser confocal system mounted on an Optiphot-2 (Tokyo, Japan) upright microscope. The confocal system was controlled through manufacturer-supplied software (ImageSpace 3.1) running on a Silicon Graphics Personal Iris 4D/35G workstation (Mountain View, CA). The 488 nm line of an argon–ion laser (high power; maximum output, 25 mW), with a 3% neutral density transmission filter (to prevent dye bleaching) was used to excite both FM1-43 and

fluo-3 dyes. Images were collected using a water-immersion lens (40×; NA, 0.75). The fluorescent images were collected every 0.5–1 sec and analyzed frame by frame with the data acquisition program of the equipment. The aperture setting of the confocal pinhole was maintained constantly in a given experiment. Images were digitized at 8 bit resolution into an array of 512 × 512 pixels.

Results

Satellite cells (MSCs): fluo-3 experiments

When 60 mM K^+ solution is substituted for the standard solution in a bath containing muscle fiber bundles from the mouse hemidiaphragm, depolarization of the fibers occurs within seconds. Some of the fibers release Ca^{2+} into the cytosol, as indicated by fluo-3 fluorescence. In regions of the muscle deemed extrajunctional by the absence of groups of postsynaptic nuclei [Fig. 1; compare with groups of nuclei at the junctional regions of fibers, immunostained (Fig. 5) and imaged for Ca^{2+} (Fig. 7, arrows)], there is very little Ca^{2+} release. In Figure 1 *A*, some peripheral "cells" show very high levels of Ca^{2+} (Fig. 1 *A*, arrows). We assess these bright areas as putative MSCs because of: (1) their peripheral position, (2) the size and shape of the putative glowing nucleus, more elongated than those of the putative myonuclei (arrowheads), (3) the paucity of apparent cytoplasm (Fig. 1*B*) compared with fibroblasts (not shown), and (4) the apparent limit of fluo-3 fluorescence, as if the area is bounded by a cell membrane. The first two criteria agree well with Schultz and McCormick's (1994) description of MSCs. Calcium transients in these cells were evident in 25 of 32 experiments performed, often in several fibers per experiment, suggesting that it is a general pattern in MSCs.

Satellite cells: fluorescence immunocytology

Confocal images of IP_3R localization give more detailed morphological evidence than the calcium imaging described above, and show in addition that these peripheral elongate structures are cells that contain IP_3Rs (Fig. 1*B*). In the projected confocal image shown in Figure 1*B*, very high concentrations (intense green) of IP_3Rs appear in specialized regions of the cytoplasm, as if there were compact organelles of smooth endoplasmic reticulum. The border between the cross-striated (dark) myofiber and the peripheral cells is clearly visible because of the comparatively higher staining for IP_3Rs in the satellite cell cytoplasm (Fig. 1*B*). We also tried to characterize these putative MSCs by position, nuclear morphology and the presence of specific markers (Figs. 2 and 3). MSC nuclei can clearly be distinguished from myonuclei (Fig. 2*A*). The elongated, rather heterochromatic nuclei of the duet MSCs of Fiber 1 are in clear contrast to the swollen, nucleolar marked myonuclei of Fiber 2 (Fig. 2*A*). The cytoplasm of the MSCs stains positively for α-actinin (Fig. 2*B*, top), which also clearly marks the Z-lines of Fiber 2. The myonuclei (see the α-actinin panel of Fig. 2*A*) are devoid of α-actinin except for a slight image of the Z-lines "under" the nuclei. Although α-actinin has not been reported as a marker for MSCs *in situ*, we have demonstrated its presence in cells known to be MSCs, using several different double labels. The first definitive evidence for such cells (at the light microscope level) being MSCs is shown in Figure 2*B*, in which the α-actinin containing MSCs, often duplex, are covered by laminin of the basal lamina. Additional evidence is that we find N-CAM, a cell adhesion molecule found as a marker in quiescent MSCs, in these peripheral cells. We also find IP_3Rs in the cells marked with N-CAM (Fig. 3*A*, arrowheads). Staining for IP_3Rs is also clear in MSCs that have been activated (Fig. 3*B*). Here, at least three nuclei (Fig. 3*B*, bottom middle) are shown

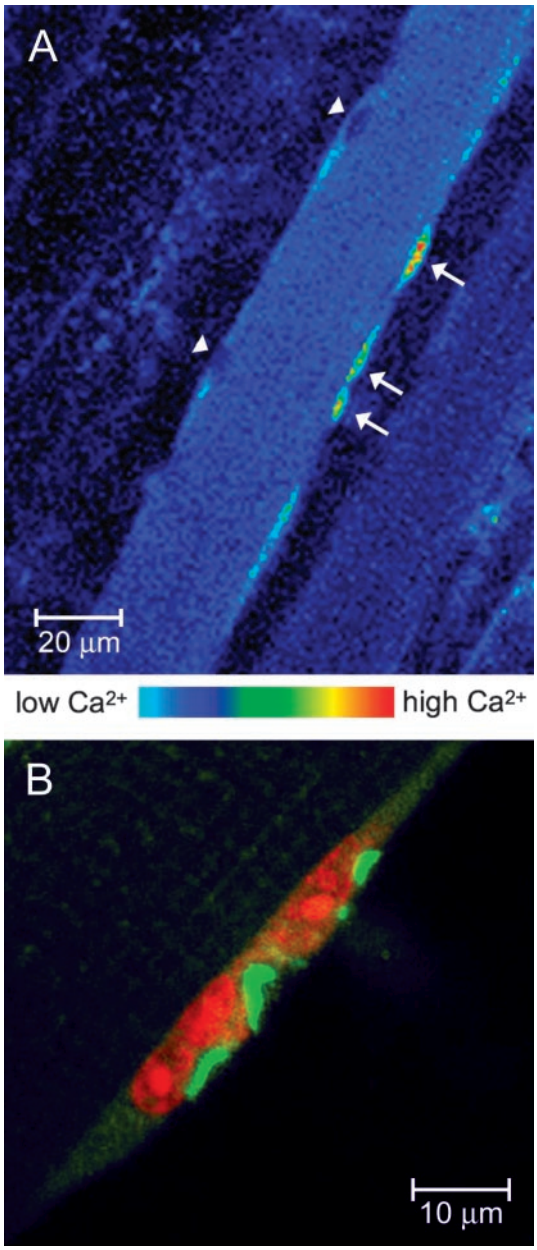

Figure 1. Intracellular calcium signals after high K^+ depolarization in putative MSCs *in situ* and immunostaining for IP_3Rs. *A*, The mouse hemidiaphragm muscle was carefully dissected and loaded with fluo-3 for 30 min at room temperature and maintained in oxygenated Krebs–Ringer's solution. Intact muscle fiber bundles were placed in a special chamber designed to fit on an upright confocal microscope. This fluorescence image was obtained 3 min after the substitution of the incubation saline by one containing 60 mM K^+ (replacing Na^+). High fluorescence can be seen in both the cytosol and nuclei of some MSCs (arrows), whereas the putative myonuclei (arrowheads) remain dark, exhibiting basal fluorescence. Thickness of optical section, 1.0 μm. *B*, Putative MSCs stain for IP_3Rs. Confocal scanning image of projected optical sections (10–15 sections, spaced 0.12 μm apart) from a whole isolated levator auris longus muscle fiber, stained for IP_3Rs (green) and for nuclei (orange) with propidium red. The morphology and position of the cells at the periphery of the fiber suggest an MSC. The fiber shows IP_3R cross-striations, as do the other adult fibers using two other different methods of fiber preparation (see Fig. 3*A*,*B*, top, and Fig. 5, right). The cytoplasmic regions of the peripheral cells are heavily stained for IP_3Rs.

that belong to cells exhibiting cytosolic desmin (Fig. 3*B*, top middle) and IP_3Rs, (Fig. 3*B*, top). Desmin is an intermediate filament specific to skeletal muscle cells and is found at the Z-line. Desmin is also specific to "activated" MSCs (Hawke and Garry, 2001);

therefore, we assume that these MSCs have been activated. In addition, these cells have the long cytoplasmic extensions characteristic of activated cells. Often, but not always, the nuclear envelope region and the nucleoplasm appear to stain positively for IP_3Rs. Control experiments blocking the IP_3R antibody with a 10× excess of peptide (see Material and Methods) show that the nucleoplasmic staining is nonspecific, whereas "envelope" staining is blocked by the peptide (Powell et al., 2001). Thus, we concur with our earlier finding that IP_3Rs are found in the I-band region of the sarcoplasmic reticulum (SR) of muscle fibers based on our interpretation of colocalizations of IP_3Rs, with both desmin (Fig. 3*B*) and α-actinin (data not shown). Colocalization in fiber striations is demonstrated clearly in Figure 3*B*, lower right, in which the overlay of IP_3R (green) and desmin (red) gives an orange to yellow-green hue.

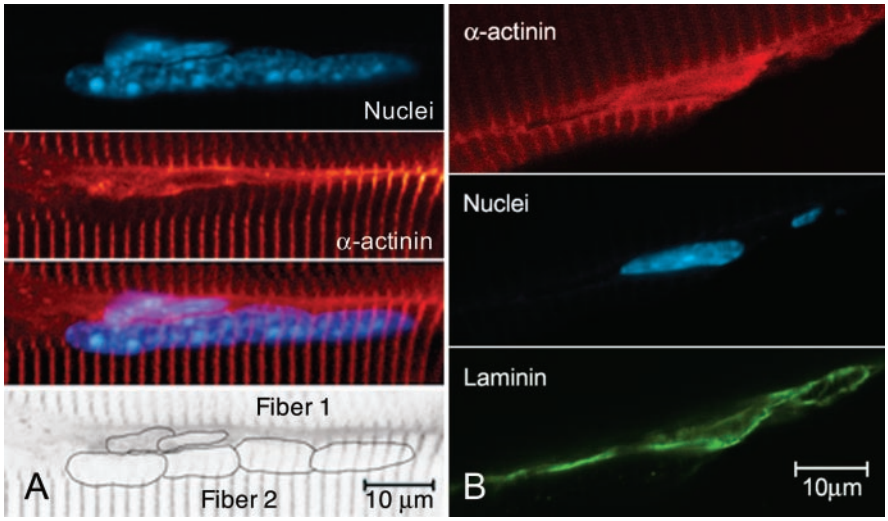

Figure 2. MSC immunostaining and myonuclei. *A*, Single optical section (0.12 μm thickness) of a 10 μm cryostat section of an adult mouse gastrocnemius muscle in a region at the edge of two fibers, showing two MSCs near the top fiber (Fiber 1) and four myonuclei in the bottom fiber (Fiber 2). Top, Position of the nuclei. Top middle, α-Actinin staining in a cross-striated pattern in the myofibers and in the cytoplasmic and perinuclear region of the MSCs of the top fiber. In Fiber 2, the area of the four myonuclei is devoid of α-actinin staining, except for the slight profile of myofibrillar staining beneath the nuclei. Only MSC cytoplasm (and nuclei) stain diffusely for α-actinin. Bottom middle, Overlay of the nuclear and α-actinin staining. Bottom, Diagram showing Fiber 1, nuclei, and Fiber 2. *B*, MSCs showing the presence of α-actinin and laminin. A single optical section (0.12 μm) of a 10 μm cryostat section of an extensor digitorum longus mouse muscle. Laminin, found in the basal lamina surrounding the MSCs, identifies the α-actinin containing cells as definitive MSCs.

Components of the NMJ

The postsynaptic endplate nuclei are transcriptionally specialized, contain specific proteins in their nuclear envelopes (Apel et al., 2000), and are easily identified by their clustering in close groups near the periphery or the center of the muscle fiber. Thus, when dissociated fibers of the mouse levator auris longus muscle were double stained for nuclei and IP_3Rs (Fig. 4, middle, inset), we could find staining that represents a tight network of IP_3Rs surrounding end plate nuclei. In fact, the organization of the IP_3R-positive region (green staining in Fig. 4, middle, inset) strongly resembles the shape of the postsynaptic gutters, marked by α-BTX binding to AChRs (Fig. 4, middle, and Fig. 5, middle). The gutters, identified by α-BTX staining, appear as projections with heavier staining on the edges (Fig. 5); the IP_3R immunostaining (Fig. 4) is very similar. Such occurrence of high levels of IP_3R is not found surrounding myonuclei outside the endplate group (Fig. 4, top, inset). At higher magnification, this prominent staining of IP_3Rs in the region corresponding to the gutters of the end plate is clear (Fig. 5, top left, asterisk). This heavy staining is partly colocalized with the AChRs as the overlay shows (Fig. 5, bottom right), the orange resulting from the overlay of the green IP_3R staining and the red α-BTX staining. Thus, the IP_3R-bearing membranes must be in very close proximity to the AChRs that are found on the crests of the postsynaptic folds (Fertuck and Salpeter, 1974, Daniels and Vogel, 1975, Flucher and Daniels, 1989).

Some of the nuclei in the endplate region have a slight accumulation of IP_3Rs in the cytoplasm surrounding them (Fig. 5, top left); we have identified these as MSCs by their position and small quantity of cytoplasm. Only the endplate nuclei seem clearly surrounded with diffuse IP_3R staining (Fig. 5, top left). Also found in Figure 5 is one nuclear area outside the "endplate basket" of nuclei (top left, arrow) very heavily stained with anti-IP_3R. This stain appears to have a discrete margin, which suggests a membrane-bound cell. This is most likely a perisynaptic (terminal) Schwann cell (PSC), based on the large amount of cytoplasm and its position outside the group of end plate nuclei. The IP_3R staining diagonal line near the "Schwann cell" is most probably the Schwann cell process, typical in both GFAP and S-100 (Schwann-cell-specific) stained specimens (Fig. 6 *A*, arrow). Labeling for PSCs with antibodies specific for Schwann cells, S-100 and GFAP (Fig. 6), give a similar picture and location. We have not yet been able to obtain good double labeling with anti-GFAP and anti-IP_3R to substantiate the assertion that the PSCs possess very high levels of IP_3R.

Calcium imaging of the mouse diaphragm fibers in the end plate region, after depolarization with high extracellular K^+, is illustrated in Figure 7. The region displayed corresponds to an NMJ, as can be inferred by the central location of the cluster of junctional nuclei (Fig. 7 *A*, JN, arrows), that clearly differ from the peripheral nuclei (Fig. 7*B*, PN, arrows), and by visualization of the motor nerve terminals by transmitted light. Also, subsequent staining with FM1-43 (data not shown) confirmed that the motor nerve indicated with an arrow in Figure 7*F*, was the axon supplying the nerve terminal innervating the superficial NMJ. The cytoplasm in the region of the subsynaptic nuclei was found to light up by 24 sec after K^+-induced membrane depolarization (Fig. 7*A*), and the area of high-calcium increases occurred first in the junctional perinuclear region (Fig. 7*A–D*), an area very similar to the one containing IP_3Rs (Figs. 4 and 5). Finally, by 72 sec (Fig. 7*E*) the calcium level increases in all nuclei.

Ca^{2+} transients in endplate regions are relatively difficult to see because of the movement artifact caused by the contracture in the high K^+ medium, which obliges to refocus the end plate region. Nine successful records in different muscles (diaphragm and levator auris longus) were performed using this method; the general pattern was usually the one shown in Figure 7.

Discussion

Satellite cells

We have identified MSCs *in situ* in adult rodent muscle at the light microscope level by their location on the periphery of the muscle fiber, by the morphology of the cell, and by the structure of the nucleus (Figs. 2*A* and 3). Such cells, when viewed with the

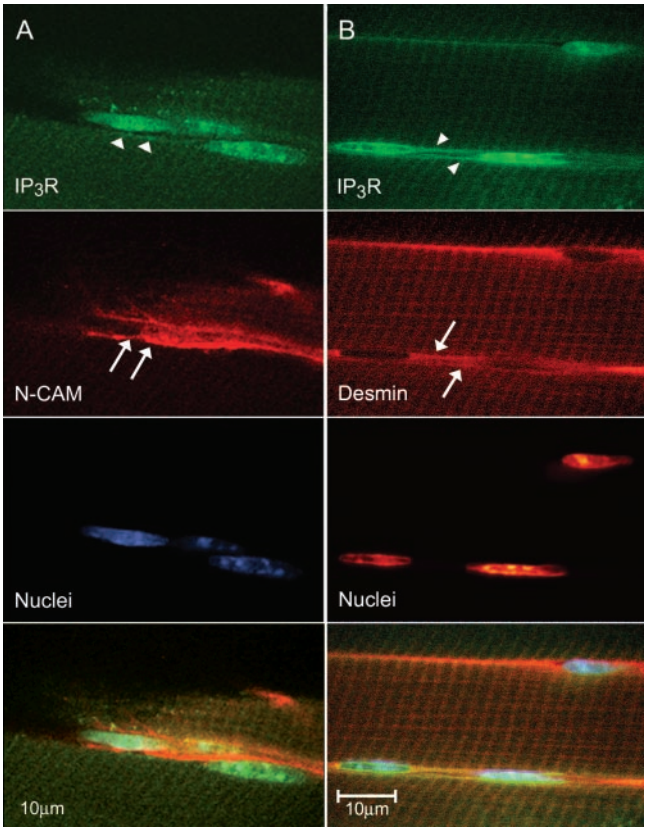

Figure 3. MSC immunostaining for IP_3Rs, N-CAM, and desmin. *A,* Confocal images of a single optical section (0.12 μm) of a 10 μm cryostat section of an extensor digitorum longus mouse muscle showing IP_3Rs in the cytoplasm (arrowheads) and N-CAM near the plasmalemma (arrows) of the cells. Bottom, Overlay of the three top panels. *B,* MSCs showing the presence of IP_3Rs and desmin. Confocal images of a single optical section (0.12 μm) of a mouse muscle as above. IP_3Rs (arrowheads) are found in cells, identified as MSCs because of the presence of desmin (arrows), an intermediate filament specific to MSCs and skeletal muscle cells. IP_3R staining exhibits cross-striations in the same regions, as does desmin staining, which is found at the Z-line. This colocalization can be seen as orange (overlay of green and red) in the bottom panel and in the cross striations in the I-band regions of the sarcomere, at the Z-line, where desmin is known to occur.

confocal microscope using fluorescence immunocytological techniques, appear to be surrounded by laminin (Fig. 2*B*), in agreement with the literature (Muir et al., 1965). In addition, these cells contain N-CAM (Fig. 3*A*) that is found in quiescent, activated, and proliferating MSCs and at the synaptic junction of adult fibers (Covault and Sanes, 1986), but not in fibroblasts or vascular tissue. Some of the MSCs contained desmin (Fig. 3*B*) which is diagnostic of activated cells (Bockhold et al., 1998); in our images these cells have long cytoplasmic extensions (Fig. 3*B*), also characteristic of activated cells. Furthermore, these cells also contain α-actinin (Fig. 2*A*,*B*), a marker not noted by Hawke and Garry (2001). However, proliferating MSCs in culture have been shown to express α-actinin, as well as vimentin and desmin (Van der Ven et al., 1992). In labeled cells of the levator auris longus muscle, the cytoplasm of these peripheral cells is packed with IP_3Rs. In double-labeled mouse extensor digitorum longus fibers, we found IP_3Rs in cells identified as MSCs by the presence of N-CAM (Fig. 3*A*) or desmin (Fig. 3*B*).

In myofibers stimulated by high K^+, we see evidence for an increase in cytoplasmic Ca^{2+} in MSCs. This calcium does not appear to come from the myofiber, but to be confined to each MSC (Fig. 1*A*). Figure 1*B* illustrates that the cytoplasm of these

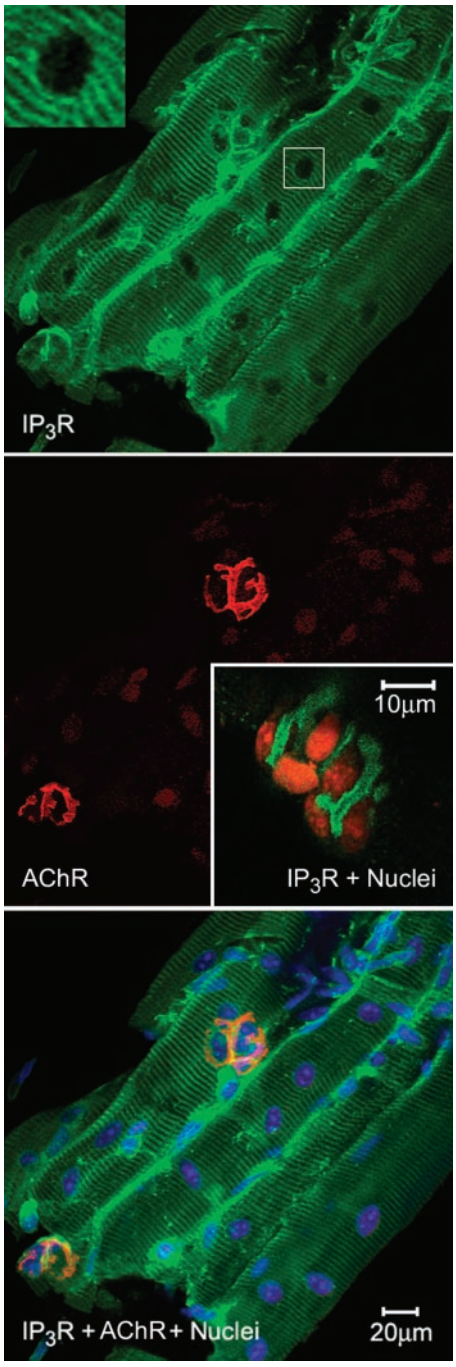

Figure 4. IP_3Rs surround endplate nuclei. Main three panels, Group of dissociated fibers from the mouse diaphragm showing IP_3R localization in a striated pattern as well as surrounding a group of nuclei (top), which are associated with the motor endplate marked by rhodaminated α-BTX, binding the AChRs (middle and bottom). Most of the myonuclei outside the motor endplate region are not surrounded by IP_3R antibody, nor is there any "corona" of IP_3R staining around the nuclei (main photo, top and inset). There are some nuclei outside the motor endplate region surrounded by IP_3Rs; these we identify by position as MSCs (see Fig. 5 for details). Middle, inset, IP_3Rs localized in the cytoplasmic regions surrounding nuclei of a motor endplate. Confocal scanning image (projection of 10–15 optical sections spaced 0.1 μm apart) from the mouse levator auris longus muscle. IP_3Rs are shown in green, and the propidium red stains the nuclei in orange. The images from this muscle suggest a very tight network of SR, in the cytoplasm enveloping the nuclei, in a region that corresponds to the morphology of the postsynaptic gutters of the NMJ. Compare with the morphology of these gutters as identified by staining with α-BTX (Fig. 4, main figure, middle and bottom, and Fig. 5). Bottom, IP_3Rs in green, nuclei in blue, and AChRs of the end plate in orange because of their close localization with IP_3R staining (see Fig. 5).

cells is full of IP_3Rs. Of course, these results with K^+ depolarization do not reveal how MSCs could become depolarized after neuromuscular activity *in situ*. It is possible that *in situ,* the K^+ concentration of the microenvironment around the MSCs could increase from a train of action potentials in the muscle fiber. This high level of K^+ could then depolarize the MSC. We have shown that a depolarization-induced IP_3 cascade in cultured muscle is triggered by the DHPR (α_1-subunit) voltage sensor (Araya et al., 2003). It is quite possible that MSCs may possess a low level of DHPR because human MSC myoblasts do show low levels of the α_1-subunit of the DHPR (Tanaka et al., 2000). If our signal transduction model for muscle in culture (Powell et al., 2001; Araya et al., 2003) holds true for the MSCs, then an IP_3 cascade would end in Ca^{2+}-dependent MSC nuclear activation. The more the particular muscle fiber contracts, the stronger the signal to the MSC, the more likely it would be recruited for proliferation and fusion with the muscle fiber. This mechanism of recruitment might be important in mild exercise (Kadi and Thornell, 2000) or in muscle growth after atrophy (Mitchell and Pavlath, 2001). Alternatively, the depolarization-induced Ca^{2+} signal could work in concert with signaling pathways triggered by growth factors and hormones.

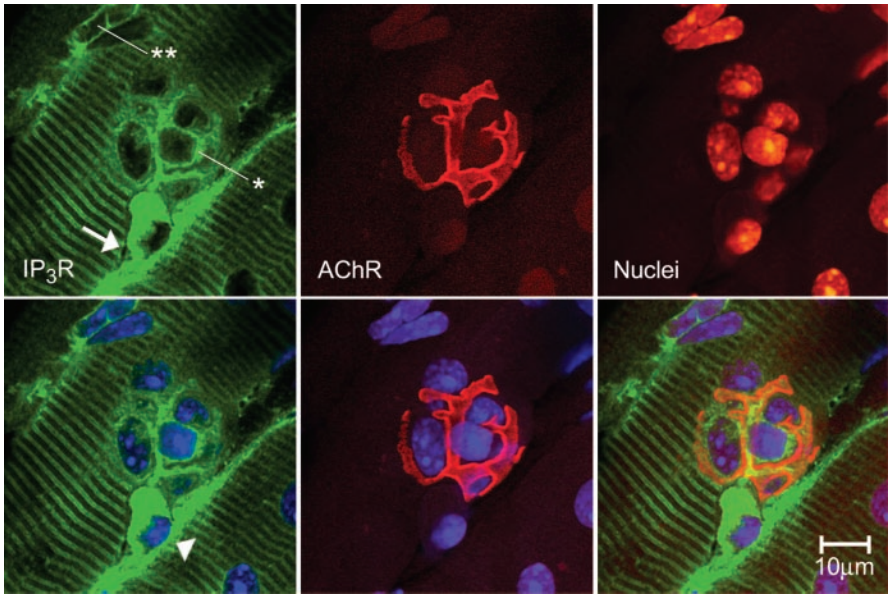

Figure 5. IP_3Rs at the motor endplate region. A more detailed view with greater resolution of part of the area shown in the main panels of Figure 4. Top, as labeled from left to right, IP_3R immunostaining as usual, is found in a striated pattern in the SR, and also surrounding the five motor endplate nuclei (also see bottom left). As can be seen in the bottom right, the heaviest IP_3R staining is found in the vicinity of AChRs of the postsynaptic gutters. A more diffuse IP_3R staining is found surrounding the endplate nuclei (*). Some other nuclei (**) are circled with IP_3Rs, and we identify these, by position, as MSCs. One other nucleus, below the group of five endplate nuclei, also seems to be surrounded by very heavy staining for IP_3Rs, the discrete margin (top left, arrow) of which suggests a membrane-bound cell. This is most likely a perisynaptic or terminal Schwann cell, on the basis of its position outside the endplate "basket" (seen clearly in the bottom right). The green diagonal line (arrowhead in the bottom left) may be the Schwann cell process (see Results). AChRs (of the postsynaptic invaginations of the end plate) are revealed by rhodamine-conjugated α-BTX binding (middle top) and with nuclei stained with TOTO-3 (middle bottom). Bottom, left to right, Image overlays: IP_3Rs and nuclei; AChRs and nuclei; IP_3Rs, nuclei, and AChRs. Note the orange color in the latter, indicating a close proximity between IP_3Rs and AChRs.

Components of the NMJ: subsynaptic nuclei and adjacent cytoplasm

The specialized nuclei of the NMJ are surrounded by IP_3Rs (Fig. 5, top left), whereas most of the extrajunctional nuclei in the myofibrillar region are not (Fig. 4, top and inset). This is probably because most extrajunctional myonuclei are transcriptionally inactive (Newlands et al., 1998). Electron microscopy images indicate that, consistent with the literature (Dauber et al., 1999, 2000), SR likely to bear receptors is found in the postsynaptic folds (data not shown); confocal images show IP_3R staining found also in the perinuclear cytoplasm (Figs. 4 and 5). Thus, IP_3Rs are positioned to respond to a release of IP_3, perhaps from the walls of the folds or from T-tubules that have been identified as continuous with the clefts, some even contributing to subsynaptic triads (Dauber et al., 2000). There are also junctions of unknown function between the subsynaptic folds and the rough SR (Dauber et al., 1999). We have found both T-tubules and diads with junctional feet at the NMJ of mouse diaphragm muscle (J. Powell and E. Pravda, unpublished results). Upon K^+ depolarization of the fluo-3-loaded mouse diaphragm muscle, Ca^{2+} seems to be released from internal stores (Fig. 7) surrounding the end plate nuclei. The signal, as soon as it can be recorded at ~20 sec after depolarization, is not found in the periphery of the myofiber, but near and then in the nuclei at these junctional sites. At extrajunctional sites, action potentials trigger increases in cytosolic Ca^{2+}, from the extracellular medium (Huang et al., 1994) or internal stores (Adams and Goldman, 1998), and cause a down-regulation of AChR, most probably via a protein kinase C pathway (Klarsfeld et al., 1989; Macpherson et al., 2002). However,

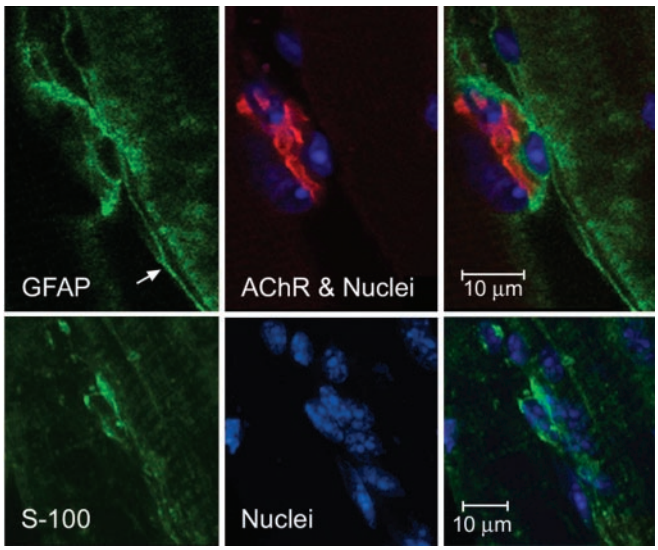

Figure 6. Immunocytochemistry for the Schwann cell and astrocyte marker GFAP and the Schwann-cell-specific marker S-100. Cells putatively identified as Schwann cells because of their positions are positive for the markers GFAP and S-100. Top, GFAP identifies as glial a cell found near the endplate nuclei of a single muscle fiber. The arrow indicates the long process of the GFAP-positive cell. Projection of 20 sections; total thickness, ~4.6 μm. Left, GFAP; middle, AChR and nuclei; right, overlay. Bottom, S-100-positive cell found near muscle cell endplate nuclei. Projection of 32 optical sections; total thickness, ~3.8 μm. Left, S-100; middle, nuclei; right, overlay. Faint cross-striations in the left panels are, we believe, nonspecific staining.

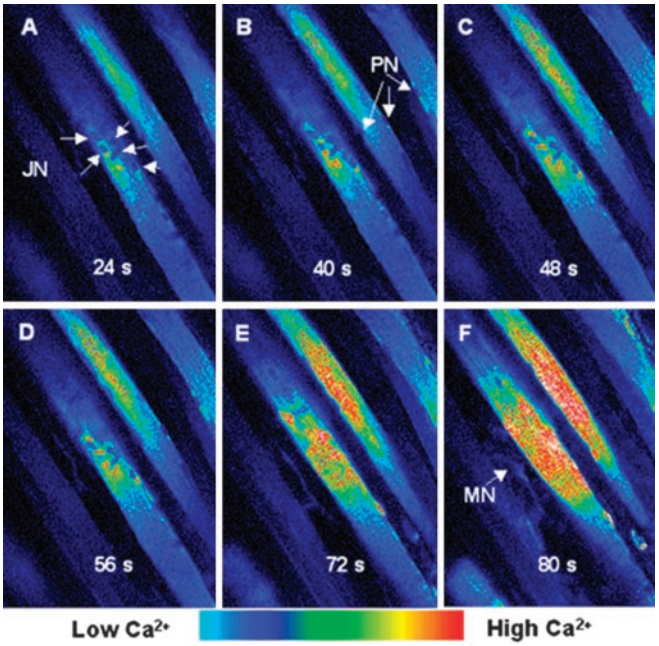

Figure 7. Intracellular calcium changes in an NMJ region after high K^+-induced depolarization. The mouse hemidiaphragm muscle bundle was carefully dissected and loaded with fluo-3 for 30 min at room temperature and maintained in oxygenated Krebs–Ringer's solution. Intact muscle fiber bundles were placed in a special chamber designed to fit on an upright confocal microscope, and fluorescence images were obtained before and after the substitution of the incubation saline by one containing 60 mM K^+ (replacing Na^+). The region on display corresponds to an NMJ, as can be inferred by the central location of junctional cluster of nuclei (*A*, JN). These nuclei differ in location from peripheral nuclei (*B*, PN). Images were acquired at the times indicated, after the addition of the high K^+ solution. A fluorescence increase in both perinuclear (*A–D*) and nuclear (*D–F*) regions is evident. A portion of the motor nerve (*F*, MN) supplying the NMJ region can also be seen.

little is known about the role of Ca^{2+} transients, such as we have seen, at the NMJ. There is some indirect evidence that Ca^{2+} influx through AChRs controls development and stabilization of the structure of the NMJ. For example, during development of the mammalian NMJ, the expression of the AChR switches from an embryonic form to an adult form, which allows more Ca^{2+} influx (Nishizaki and Sumikawa, 1994; Villarroel and Sakmann, 1996); the lack of this switch can prevent normal development of the NMJ (Engel et al., 1996).

At the NMJ a slow Ca^{2+} transient, not accompanied by contraction, and similar to what we see with K^+-induced depolarization, is generated by motor nerve stimulation (Dezaki et al., 1997). This intracellular calcium appears to regulate agrin-induced AChR clustering and maintenance of clusters in cultured myotubules (Megeath and Fallon, 1998). We suggest that the AChR channel may not be the only source of the Ca^{2+} transient, but that the IP_3Rs, found at the NMJ–SR, may also release Ca^{2+}. Because we have demonstrated in cultured muscle that K^+ depolarization triggers IP_3 release as a response to the DHPR voltage-sensor via a G-protein (Araya et al., 2003) as part of a signaling cascade likely to regulate early gene expression (Carrasco et al., 2003), we propose that a similar mechanism may occur in adult muscle fibers. It has been shown recently (Salanova et al., 2002) that adult muscle fibers have the same pattern of type-1 IP_3 receptors we described for cultured myotubules (Powell et al., 2001); unlike myotubules, most muscle fiber nuclei appear devoid of perinuclear IP_3Rs, so such a mechanism for regulation of gene expression may be particularly important for the NMJ.

Components of the NMJ: PSCs

In most of our confocal images of mouse NMJ stained for IP_3Rs, one to three PSCs containing IP_3Rs were identified capping the regions of the nerve ending (Fig. 5). These cells were identified as PSCs because of their position beyond (on top of) the postsynaptic nuclei of the endplate "basket," by their abundant cytoplasm apparently bounded by a discrete margin (membrane), and by typical process extensions along the margin of the muscle fiber. These characteristics were also found in PSCs identified by staining with antibodies to Schwann-cell-specific proteins (S-100 and GFAP).

PSCs have at least three major functions: (1) modulation of nerve growth in development (Herrera et al., 2000), (2) enhancement of directional nerve growth in synapse regeneration (Balice-Gordon, 1996), and (3) synaptic maintenance (Robitaille, 1998) that is probably mediated through adjusting the efficacy of the synapse by regulating transmitter release (Robitaille, 1998; Castonguay and Robitaille, 2001). Nerve activity allows the continued secretion of ACh, which binds to the muscarinic AChRs of the PSC. The consequent depolarization leads to Ca^{2+} transients in the PSC, resulting in a modulation of ACh release (Rochon et al., 2001). The Ca^{2+} comes from internal stores, and the time sequence is in the time domain of slow IP_3-driven Ca^{2+} transient in cultured skeletal muscle (Jaimovich et al., 2000, Powell et al., 2001). In the latter case, we have outlined a signal transduction cascade that ends in the upregulation of early genes (Jaimovich and Carrasco, 2002, Araya et al., 2003). Because we have found such high levels of IP_3Rs in the PSCs, we suggest that the calcium transients in these cells are also in an IP_3 cascade. What the molecular consequences of this signal may be is, of course, unknown.

There is no question that more experimentation is necessary to secure all the details of this model of IP_3 control of MSC activation and contribution to fiber growth, and NMJ stabilization, but we believe these findings can be the foundation for additional research, the results of which will lead to a broader understanding of Ca^{2+} signaling at the neuromuscular junction and in skeletal muscle.

References

Adams L, Goldman D (1998) Role for calcium from the sarcoplasmic reticulum in coupling muscle activity to nicotinic acetylcholine receptor gene expression in rat. J Neurobiol 35:245–257.

Apel ED, Lewis RM, Grady RM, Sanes JR (2000) Syne-1, a dystrophin- and Klarsicht-related protein associated with synaptic nuclei at the neuromuscular junction. J Biol Chem 275:31986–31995.

Araya R, Liberona JL, Riveros N, Powell JA, Carrasco MA, Jaimovich E (2003) Dihydropyridine receptors as voltage sensors for the depolarization-evoked slow calcium signal in skeletal muscle cells. J Gen Physiol 121:3–16.

Balice-Gordon RJ (1996) Dynamic roles at the neuromuscular junction: Schwann cells. Curr Biol 6:1054–1056.

Betz WJ, Mao F, Bewick GS (1992) Activity-dependent fluorescent staining and destaining of living vertebrate motor nerve terminals. J Neurosci 12:363–375.

Bhasin S, Storer TW, Berman N, Callegari C, Clevenger B, Phillips J, Bunnell TJ, Tricker R, Shirazi A, Casaburi R (1996) The effects of supraphysiologic doses of testosterone on muscle size and strength in normal men. N Engl J Med 335:1–7.

Bischoff R (1997) Chemotaxis of skeletal muscle satellite cells. Dev Dyn 208:505–515.

Bockhold KJ, Rosenblatt JD, Partridge TA (1998) Aging normal and dystrophic mouse muscle: analysis of myogenicity in cultures of living single fibers. Muscle Nerve 21:173–183.

Brevet A, Pinto E, Peacock J, Stockdale FE (1976) Myosin synthesis increased by electrical stimulation of skeletal muscle cell cultures. Science 193:1152–1154.

Carrasco MA, Riveros N, Ríos J, Müller M, Torres F, Pineda J, Lantadilla S, Jaimovich E (2003) Depolarization induced slow calcium transients activate early genes in skeletal muscle cells. Am J Physiol Cell Physiol 284:C1438–C1447.

Castonguay A, Robitaille R (2001) Differential regulation of transmitter release by presynaptic and glial Ca^{2+} internal stores at the neuromuscular synapse. J Neurosci 21:1911–1922.

Covault J, Sanes JR (1986) Distribution of NCAM in synaptic and extrasynaptic portions of developing and adult skeletal muscle. J Cell Biol 102:716–730.

Daniels MP, Vogel Z (1975) Immunoperoxidase staining of alpha-bungarotoxin binding sites in muscle end plates shows distribution of acetylcholine receptors. Nature 254:339–341.

Dauber W, Voigt T, Heini A (1999) Junctions between subsynaptic folds and rough sarcoplasmic reticulum of muscle fibres. J Muscle Res Cell Motil 20:697–701.

Dauber W, Voigt T, Hartel X, Mayer J (2000) The T-tubular network and its triads in the sole plate sarcoplasm of the motor end-plate of mammals. J Muscle Res Cell Motil 21:443–449.

Dezaki K, Tsuneki H, Kimura I (1997) Slow Ca^{2+} (RAMIC) mobilization operated by postsynaptic neuronal nicotinic receptor regulates synaptic function at the mouse neuromuscular junction. Nippon Yakurigaku Zasshi 110 Suppl 1:114P–119P.

Dolmetsch RE, Lewis RS, Goodnow CC, Healy JI (1997) Differential activation of transcription factors induced by Ca^{2+} response amplitude and duration. Nature 386:855–858.

Doumit ME, Cook DR, Merkel RA (1993) Fibroblast growth factor, epidermal growth factor, insulin-like growth factors, and platelet-derived growth factor-BB stimulate proliferation of clonally derived porcine myogenic satellite cells. J Cell Physiol 157:326–332.

Dunn SE, Chin ER, Michel RN (2000) Matching of calcineurin activity to upstream effectors is critical for skeletal muscle fiber growth. J Cell Biol 151:663–672.

Engel AG, Ohno K, Milone M, Wang HL, Nakano S, Bouzat C, Pruitt JN, Hutchinson DO, Brengman JM, Bren N, Sieb JP, Sine SM (1996) New mutations in acetylcholine receptor subunit genes reveal heterogeneity in the slow-channel congenital myasthenic syndrome. Hum Mol Genet 5:1217–1227.

Fertuck HC, Salpeter MM (1974) Localization of acetylcholine receptors by ^{125}I-labeled alpha-bungarotoxin binding at mouse motor end plates. Proc Natl Acad Sci USA 71:1376–1378.

Flucher BE, Daniels MP (1989) Distribution of Na^+ channels and ankyrin in neuromuscular junctions is complementary to that of acetylcholine receptors and the 43 kD protein. Neuron 3:163–175.

Haugk KL, Roeder RA, Garber MJ, Schelling GT (1995) Regulation of muscle cell proliferation by extracts from crushed muscle. J Anim Sci 73:1972–1981.

Hawke TJ, Garry DJ (2001) Myogenic satellite cells: physiology to molecular biology. J Appl Physiol 91:534–551.

Herrera AA, Qiang H, Ko CP (2000) The role of perisynaptic Schwann cells in development of neuromuscular junctions in the frog (*Xenopus laevis*). J Neurobiol 45:237–254.

Huang CF, Flucher BE, Schmidt MM, Stroud SK, Schmidt J (1994) Depolarization-transcription signals in skeletal muscle use calcium flux through L channels, but bypass the sarcoplasmic reticulum. Neuron 13:167–177.

Jaimovich E, Carrasco MA (2002) IP_3 dependent Ca^{2+} signals from the cell membrane to the nucleus of muscle cells are involved in regulation of gene expression. Biol Res 35:195–202.

Jaimovich E, Rojas E (1994) Intracellular Ca^{2+} transients induced by high external K^+ and tetracaine in cultured rat myotubes. Cell Calcium 15:356–368.

Jaimovich E, Reyes R, Liberona JL, Powell JA (2000) IP_3 receptors, IP_3 transients, and nucleus-associated Ca^{2+} signals in cultured skeletal muscle. Am J Physiol Cell Physiol 278:C998–C1010.

Kadi F, Thornell LE (2000) Concomitant increases in myonuclear and satellite cell content in female trapezius muscle following strength training. Histochem Cell Biol 113:99–103.

Klarsfeld A, Laufer R, Fontaine B, Devillers-Thiery A, Dubreuil C, Changeux JP (1989) Regulation of muscle AChR alpha subunit gene expression by electrical activity: involvement of protein kinase C and Ca^{2+}. Neuron 2:1229–1236.

Liberona JL, Powell JA, Shenoi S, Petherbridge L, Caviedes R, Jaimovich E (1998) Differences in both inositol 1,4,5-trisphosphate mass and inositol 1,4,5-trisphosphate receptors between normal and dystrophic skeletal muscle cell lines. Muscle Nerve 21:902–909.

Macpherson P, Kostrominova T, Tang H, Goldman D (2002) Protein kinase C and calcium/calmodulin-activated protein kinase II (CaMK II) suppress nicotinic acetylcholine receptor gene expression in mammalian muscle: a specific role for CaMK II in activity-dependent gene expression. J Biol Chem 277:15638–15646.

Megeath LJ, Fallon JR (1998) Intracellular calcium regulates agrin-induced acetylcholine receptor clustering. J Neurosci 18:672–678.

Mitchell PO, Pavlath GK (2001) A muscle precursor cell-dependent pathway contributes to muscle growth after atrophy. Am J Physiol Cell Physiol 281:C1706–C1715.

Moschella MC, Watras J, Jayaraman T, Marks AR (1995) Inositol 1, 4, 5-trisphosphate receptor in skeletal muscle: differential expression in myofibres. J Muscle Res Cell Motil 16:390–400.

Muir AR, Kanji AH, Allbrook D (1965) The structure of the satellite cells in skeletal muscle. J Anat 99:435–444.

Newlands S, Levitt LK, Robinson CS, Karpf AB, Hodgson VR, Wade RP, Hardeman EC (1998) Transcription occurs in pulses in muscle fibers. Genes Dev 12:2748–2758.

Nishizaki T, Sumikawa K (1994) A cAMP-dependent Ca^{2+} signalling pathway at the end plate provided by the gamma to epsilon subunit switch in ACh receptors. Brain Res Mol Brain Res 24:341–345.

Pallafacchina G, Calabria E, Serrano AL, Kalhovde JM, Schiaffino S (2002) A protein kinase B-dependent and rapamycin-sensitive pathway controls skeletal muscle growth but not fiber type specification. Proc Natl Acad Sci USA 99:9213–9218.

Powell JA, Carrasco MA, Adams DS, Drouet B, Rios J, Muller M, Estrada M, Jaimovich E (2001) IP(3) receptor function and localization in myotubes: an unexplored Ca^{2+} signaling pathway in skeletal muscle. J Cell Sci 114:3673–3683.

Ribchester RR, Mao F, Betz WJ (1994) Optical measurements of activity-dependent membrane recycling in motor nerve terminals of mammalian skeletal muscle. Proc R Soc Lond B Biol Sci 255:61–66.

Robitaille R (1998) Modulation of synaptic efficacy and synaptic depression by glial cells at the frog neuromuscular junction. Neuron 21:847–855.

Rochon D, Rousse I, Robitaille R (2001) Synapse–glia interactions at the mammalian neuromuscular junction. J Neurosci 21:3819–3829.

Salanova M, Priori G, Barone V, Intravaia E, Flucher B, Ciruela F, Mcllhinney RAJ, Parys JB, Mikoshiba K, Sorrentino V (2002) Homer proteins and $InsP_3$ receptors co-localise in the longitudinal sarcoplasmic reticulum of skeletal muscle fibres. Cell Calcium 32:193–200.

Sanes JR, Lichtman JW (1999) Development of the vertebrate neuromuscular junction. Annu Rev Neurosci 22:389–442.

Schaeffer L, de Kerchove d'Exaerde A, Changeux JP (2001) Targeting transcription to the neuromuscular synapse. Neuron 31:15–22.

Schultz E, McCormick KM (1994) Skeletal muscle satellite cells. Rev Physiol Biochem Pharmacol 123:213–257.

Tanaka H, Furuya T, Kameda N, Kobayashi T, Mizusawa H (2000) Triad proteins and intracellular Ca^{2+} transients during development of human skeletal muscle cells in aneural and innervated cultures. J Muscle Res Cell Motil 21:507–526.

Trachtenberg JT, Thompson WJ (1997) Nerve terminal withdrawal from rat neuromuscular junctions induced by neuregulin and Schwann cells. J Neurosci 17:6243–6255.

Van der Ven PF, Schaart G, Jap PH, Sengers RC, Stadhouders AM, Ramaekers FC (1992) Differentiation of human skeletal muscle cells in culture: maturation as indicated by titin and desmin striation. Cell Tissue Res 270:189–198.

Villarroel A, Sakmann B (1996) Calcium permeability increase of end plate channels in rat muscle during postnatal development. J Physiol (Lond) 496:331–338.